molecular pharmaceutics

Article

pubs.acs.org/molecularpharmaceutics

Redox-Responsive Polymer–Drug Conjugates Based on Doxorubicin and Chitosan Oligosaccharide-*g*-stearic Acid for Cancer Therapy

Yigang Su,[†,§] Yingwen Hu,[†,§] Yongzhong Du,[†] Xuan Huang,[‡] Jiabei He,[†] Jian You,[†] Hong Yuan,[†] and Fuqiang Hu*[,†]

[†]College of Pharmaceutical Sciences, Zhejiang University, Yuhangtang Road 866, Hangzhou 310058, People's Republic of China

[‡]Department of Pharmacy, School of Medicine Science, Jiaxing University, Jiaxing, Zhejiang 314001, People's Republic of China

Supporting Information

ABSTRACT: Here, a biodegradable polymer–drug conjugate of doxorubicin (DOX) conjugated with a stearic acid-grafted chitosan oligosaccharide (CSO-SA) was synthesized via disulfide linkers. The obtained polymer–drug conjugate DOX-SS-CSO-SA could self-assemble into nanosized micelles in aqueous medium with a low critical micelle concentration. The size of the micelles was 62.8 nm with a narrow size distribution. In reducing environments, the DOX-SS-CSO-SA could rapidly disassemble result from the cleavage of the disulfide linkers and release the DOX. DOX-SS-CSO-SA had high efficiency for cellular uptake and rapidly released DOX in reductive intracellular environments. *In vitro* antitumor activity tests showed that the DOX-SS-CSO-SA had higher cytotoxicity against DOX-resistant cells than free DOX, with reversal ability up to 34.8-fold. DOX-SS-CSO-SA altered the drug distribution *in vivo*, which showed selectively accumulation in tumor and reduced nonspecific accumulation in hearts. *In vivo* antitumor studies demonstrated that DOX-SS-CSO-SA showed efficient suppression on tumor growth and relieved the DOX-induced cardiac injury. Therefore, DOX-SS-CSO-SA is a potential drug delivery system for safe and effective cancer therapy.

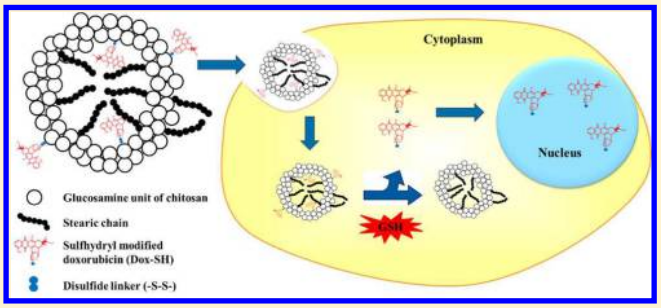

KEYWORDS: *redox-responsive, polymer–drug conjugates, controlled release, chitosan, drug resistance*

1. INTRODUCTION

Over the past 20 years, polymer–drug conjugates have attracted abundant attention and several of them are currently under clinical investigation as controlled drug delivery systems for anticancer therapy.[1,2] Usually, a polymer–drug conjugate consists of a hydrophilic polymer and a hydrophobic drug, which are joined via chemical linkers. Chemically conjugating drugs onto polymer not only benefits the polymer micelles but also effectively prevents drug leaking into the circulation.[3]

Smart polymer–drug conjugate is a prodrug, which remains inactive in systemic circulation and releases activated drugs in response to specific stimuli at the target sites, such as temperature, pH, redox potential, light, and enzymes.[4−9] Among the stimuli, redox potential is often used to trigger the intracellular drug delivery.[4,10,11] In the human body, the intracellular concentration of reduced substances is on average 1−11 mM, but only 1−10 μM in fluids outside cells, such as plasma. In addition, the intracellular thiol concentration is much higher in cancer cells than corresponding normal tissues.[12,13] Disulfide bonds (−S−S−) have great biological value, which can be cleaved into thiols via abundant reducing substances, including glutathione (GSH).[14] This phenomenon provides an opportunity for triggered drug to release from disulfide-linked polymer–drug conjugates within the tumor cells.

Doxorubicin (DOX) is widely used for the treatment of various tumors, including hematological malignancies, soft tissue sarcomas, and many others. The exact action mechanism of DOX remains unclear, but generally accepted that it interacts with DNA through intercalation and inhibits topoisomerase II. Despite its high antitumor activity, DOX is limited in the clinical application due to severe side effects and multiple drug resistance (MDR). DOX induces cytotoxicity in normal tissue and cardiotoxicity with a lack of specific biodistribution.[15] In MDR carcinoma cells, overexpression of P-glycoprotein (P-gp) can lead to efflux of the drug from cells.[16]

In previous studies, we have synthesized glycolipid-like copolymer based on chitosan oligosaccharide (CSO) and stearic acid (SA).[17] The obtained chitosan oligosaccharide copolymer (CSO-SA) has a stable physicochemical property, which is widely developed for drug delivery, including chemicals and genetic drugs.[18−21] Moreover, CSO-SA can be internalized into cells excellently attributed to the hydrophobic microdomains near the surface of the micelles.[18] However, along with many copolymers, the drug release rate of CSO-SA

Received: October 23, 2014
Revised: January 27, 2015
Accepted: March 9, 2015
Published: March 9, 2015

DOI: 10.1021/mp500710x
Mol. Pharmaceutics 2015, 12, 1193−1202

was relatively slow according to the *in vitro* drug release assay, resulting from the slow degradation of the amide linkages between the hydrophilic shell and the hydrophobic core. Thus, polymer−drug conjugates with DOX attached to CSO-SA via a disulfide linkage responding to intracellular high concentrations of GSH might be a feasible approach for triggered drug release.

In this study, we present a polymer−drug conjugate system for anticancer drug delivery and redox-triggered drug release. When polymer−drug conjugate passively targeted the solid tumor tissue and was internalized by tumor cells, DOX was released from the micelles due to cleavage of disulfide linkers in response to the reductive intracellular microenvironment and trans-located into nuclei to take effect. Doxorubicin base (DOX), as a model antitumor drug, was covalently conjugated to the backbone of the CSO-SA micelles via disulfide bonds to form redox-responsive doxorubicin−S−S−chitosan oligosaccharide−*g*-stearic acid conjugate micelles. The characteristics, *in vitro* drug release behavior in a reductive environment and the cytotoxicity were then investigated. *In vivo* experiments were conducted to confirm the passive targeting ability and the antitumor activities of DOX-SS-CSO-SA.

2. MATERIALS AND METHODS

2.1. Materials and Animals. Chitosan oligosaccharide (M_w =17.5 kDa, 95% deacetylated degree) was obtained by enzymatic degradation from chitosan (M_w = 450.0 kDa), which was supplied by Yuhuan Marine Biochemistry Co., Ltd. (Zhejiang, China).[22] Stearic acid (SA) was purchased from Chemical Reagent Co., Ltd. (Shanghai, China). 1-Ethyl-3-(3-(dimethylamino)propyl) carbodiimide (EDC) was purchased from Shanghai Medpep Co., Ltd. (Shanghai, China). Doxorubicin hydrochlorate (DOX·HCl) was a gift from Hisun Pharm Co., Ltd., China. Fluorescein isothiocyanate (FITC), and 3-(4,5-dimethyl-thiazol-2-yl)-2,5 -diphenyl-tetrazolium bromide (MTT) were purchased from Sigma (St. Louis, MO, USA). Dithiobis (succinimidyl propionate) (DSP) was obtained from Tokyo Chemical Industry Co., Ltd. (Tokyo, Japan). Pyrene was purchased from Aldrich Chemical Co. (USA). 1,1′-Dioctadecyl-3,3,3′,3′-tetramethylindotricarbocyanine iodide (DiR) was a product of Molecular Probes, Inc. (Eugene, OR, USA). Dulbecco's modified Eagle's medium (DMEM) and trypsin-EDTA were purchased from Gibco-BRLC (MD, USA). Fetal bovine serum (FBS) was purchased from Sijiqing Biologic Co., Ltd. (Zhejiang, China). Commercial doxorubicin hydrochloride injection was obtained from Pfizer (USA). All other chemicals were of analytical or chromatographic grade.

Male BALB/C nude mice (6−8 weeks old) were purchased from Shanghai SLAC Laboratory Animal Co., Ltd. (Shanghai, China). All animal studies were performed under Institutional Animal Care and Use Committee-approved protocols.

2.2. Synthesis of CSO-SA. As previously reported, CSO-SA was synthesized by a one-step reaction. We used the carboxyl group of SA reacting with the free amino groups of CSO by an amine-reactive coupling, which was catalyzed by EDC.[17,21] Briefly, 1.0 g of CSO (M_w = 17.5 *k*Da) was dissolved in 60 mL of DI water. A total of 1.65 g of SA and 11.0 g of EDC was dissolved in ethanol and activated at 60 °C for 30 min. Then the ethanol solution was added dropwise into the chitosan solution with stirring at 80 °C for 4 h. The reactant mixtures were dialyzed with a dialysis membrane (MWCO 7000 Da) against DI water for 2 days followed by freeze-drying. The lyophilized product was washed with ethanol to remove unreacted reagent. Finally, the product was redispersed in deionized water and lyophilized, and the CSO-SA were received.

2.3. Synthesis of DOX-Conjugated CSO-SA (DOX-SS-CSO-SA). Doxorubicin hydrochloride (DOX·HCl) was reacted with triethylamine in dimethyl sulfoxide overnight to produce the DOX.[23] DOX was conjugated to CSO-SA micelles via disulfide links to dithiobis (succinimidyl propionate) (DSP) in two reaction steps. All reactions were under dark conditions.

DOX and DSP were dispersed in DMSO. DOX/DMSO solution (20 mg/mL) was added dropwise to 20 mg/mL DSP/DMSO solution (DOX/DSP = 1:1, molar ratio). A catalytic amount of triethylamine (0.5 μL) was added into the reaction mixture under stirring for 2 h at room temperature. The reactant mixture was dialyzed (MWCO 3000 Da) against DI water for 24 h followed by freeze-drying to obtain the DOX-DSP intermediates.

Then a certain weight of CSO-SA was dissolved in DI with ultrasonic dispersion uniformity to form a micelle solution. The pH of the solution was adjusted to 7.4. DOX-DSP was dissolved in DMSO to a concentration of 10 mg/mL and added to the CSO-SA micelle solution in drops (DOX/CSO-SA = 1:10, w/w). The solution was stirred for 12 h and then dialyzed against DI water (MWCO 7000 Da) for 48 h followed by freeze-drying. Afterward, the lyophilized product was washed thrice with DMSO to remove unreacted DOX-DSP molecules. Then the solution was lyophilized and the DOX-SS-CSO-SA was obtained.

2.4. Physicochemical of CSO-SA and DOX-SS-CSO-SA.

2.4.1. ^{1}H NMR Analysis. The ^{1}H NMR spectra of the chemicals were used to verify the chemical structures. The chemicals were dissolved in 20.0 mg/mL of dimethyl sulfoxide-d_6 or D_2O.

2.4.2. LC/MS Analysis. The reaction mixture was transferred into a sample vial and analyzed by LC/MS.

LC/MS analysis: Agilent 1200 Series UPLC and 6460 Series mass spectrometers were used (Agilent Technologies, Palo Alto, CA, USA). Mobile phase: methanol/0.01 M ammonium acetate/acetic acid = 68:30:3 (v/v/v).

HPLC analysis was performed at a flow rate of 0.8 mL/min. Mass spectra were acquired in positive ion modes.

2.4.3. SA Content in CSO-SA. SA content in CSO-SA was determined by the 2,4,6-trinitrobenzenesulfonic acid (TNBS) method. 0.3 mL of CSO-SA solution at 1 mg/mL was incubated with 2.0 mL $NaHCO_3$ (4.0%) and 2.0 mL of TNBS (0.1%) at 37 °C for 2 h. Then 2.0 mL of HCl (2 mol/L) was added and the results were measured at 344 nm by an ultraviolet spectrophotometer. The degree of SA in CSO-SA is calculated by the following formula:

$$\frac{A_{CSO}}{A_{CSO-SA}} = \frac{M_{CSO-SA}}{M_{CSO}} \times \frac{n_{NH2}}{n_{NH2} - m_{NH2}}$$

where A_{CSO} is the UV absorbance of CSO, $A_{CSO\text{-}SA}$ is the UV absorbance of CSO-SA, $M_{CSO\text{-}SA}$ is the molecular weight of CSO-SA, M_{CSO} is the molecular weight of CSO, n_{NH2} is the total number of moles of $-NH_2$ in the CSO chain, and m_{NH2} is the content of SA on CSO.

2.4.4. DOX Content in DOX-SS-CSO-SA. We used an ultraviolet spectrophotometer (DU640, Beckman-Counter, USA) to measure the DOX content in DOX-SS-CSO-SA.[24] DOX and DOX-SS-CSO-SA were dispersed in a mixture of DMSO and H_2O (5:95, v/v), and the DOX content was calculated compared to a standard curve obtained using DOX.

DOI: 10.1021/mp500710x
Mol. Pharmaceutics 2015, 12, 1193−1202

2.4.5. Critical Micelle Concentration. To measure the critical micelle concentration (CMC) of DOX-SS-CSO-SA, pyrene was used as a probe and detected by the fluorescence spectroscopy.[25] To determine the intensity ratio (I_1/I_3) of the first peak (I_1, 374 nm) to the third peak (I_3, 385 nm) in the pyrene emission spectra, sample solutions of different concentrations containing pyrene (5.93×10^{-7} mol/L) were excited at 337 nm, and the emission spectrum of pyrene was obtained in the range of 360−450 nm with a fluorometer (F-2500, Hitachi Co., Japan). The slit openings for excitation and emission were at 10.0 and 2.5 nm, respectively.

2.4.6. Particle Size and Zeta Potential. The sizes of the micelles with CSO-SA were detected by dynamic light scattering (DLS) using a Zetasizer (Malvern Instrument Ltd.). The zeta potential was also measured by the Zetasizer.

2.4.7. Morphology of Particles. The morphology examinations were performed by TEM (JEOL JEM-1230, Japan). The samples were placed on carbon-coated copper grids and stained with 2% (w/v) phosphotungstic acid.

2.5. Redox-Responsive Behaviors and *in Vitro* DOX Release. To demonstrate that the disulfide bonds are cleavable and DOX was quickly released from micelles in the reductive environment, DOX-SS-CSO-SA micelles were dissolved in PBS (pH, 7.4) containing 10 mM or 10 μM dithiothreitol (DTT) at a drug concentration of 5 μg/mL. The fluorescence intensity was scanned at different time points (0−50 min) using a fluorescence spectrometer with an excitation wavelength of 505 nm. Additionally, the fluorescence intensity of DOX at the same concentration was detected under the same conditions as the control.

The *in vitro* release profile of DOX from DOX-SS-CSO-SA micelles was investigated by dialysis in PBS (pH 7.4) medium containing 10 mM or 10 μM DTT. The DOX-SS-CSO-SA containing 100 μg of DOX was dialyzed against 20 mL of buffer (MWCO 7000 Da). At the designated time points, the media was collected and replaced with fresh medium. Drug concentrations were measured by fluorometer (Em = 505 nm; Ex = 565 nm) and calculated in comparison with a standard curve. Free DOX was performed under the same conditions as a control. All release tests were performed in triplicate.

2.6. Cell Culture. Human breast cancer MCF-7 cells and multidrug resistant variant MCF-7/ADR cells were gifts from the first Affiliated Hospital, College of Medicine, Zhejiang University. Human liver tumor BEL-7402 cells were obtained from the Institute of Biochemistry and Cell Biology. Cells were cultured in Dulbecco's modified Eagle's medium (DMEM) supplemented with 10% (v/v) fetal bovine serum (FBS) in a humidified atmosphere containing 5% CO_2 at 37 °C. Cells were regularly subcultured using trypsin/ethylenediaminetetraacetic acid (EDTA).

2.7. Internalization and Intracellular Trafficking of DOX-SS-CSO-SA Micelles. DOX-SS-CSO-SA micelles were labeled with fluorescein isothiocyanate (FITC) via the amino group of chitosan and the isothiocyanate group of FITC. Cells were transferred and cultured on 20 mm cover glass in a 24-well plate at 1.0×10^5 mL^{-1} cells/well and allowed to grow for 24 h. DOX·HCl and FITC-labeled DOX-SS-CSO-SA micelles of a certain concentration (DOX content was 5 μg/mL) were added. After different incubation periods, cell nuclei were stained with Hoechst 33342. Cell monolayers on cover glasses were repeatedly rinsed with PBS and mounted for microscopic examination. A confocal laser scanning microscope (Olympus, Japan) was used to image the intracellular fluorescence. For a quantitative study, cells were harvested and resuspended in PBS. The intensity of cellular fluorescence was determined by flow cytometer (FC500MCL, Beckman Coulter).

2.8. *In Vitro* Antitumor Activity. A cytotoxicity comparison was performed using BEL-7402, MCF-7, and MCF-7/ADR cells with *in vitro* proliferation using the MTT method. Briefly, cells were seeded at 1.0×10^4 mL^{-1} cells/well in a 96-well plate (Nalge Nunc International, Naperville, IL, USA) and allowed to grow for 24 h. After treating DOX·HCl, DOX, CSO-SA, and DOX-SS-CSO-SA micelles with a series of concentrations, the cells were further cultured for 48 h. Then, 20 μL of MTT solution (5 mg/mL) was added. After incubating for an additional 4 h at 37 °C, the medium was removed, and 200 μL of DMSO was added into each well for dissolution of the MTT formazan crystals. Finally, the absorbance at 570 nm was measured by a microplate reader (Bio-Rad, Model 680, USA). All experiments were performed in triplicate. The overcome ratio of drug resistance was calculated from formula 1:[20,26]

$$\text{overcome power} = (R_f/R_m)/(S_f/S_m) \quad (1)$$

where R_f was the IC_{50} value of the drug against the drug-resistant cells; R_m was the IC_{50} value of DOX-SS-CSO-SA micelles against the drug resistant cells; S_f was the IC_{50} value of the drug against drug-sensitive cells; and S_m was the IC_{50} value of the DOX-SS-CSO-SA micelles against the drug-sensitive cells.

2.9. *In Vivo* Distribution. To prepare the tumor-bearing mice models, a tumor cell suspension of approximately 1.0×10^7 BEL-7402 cells was inoculated subcutaneously in the BALB/C nude mice (6−8 weeks). To investigate the *in vivo* distribution, DOX-SS-CSO-SA micelles was labeled with the near-infrared dye DiR. DiR/DMSO stock solution was slowly added dropwise into DOX-SS-CSO-SA micelle solution. After stirring for 1 h, the mixture was ultrasonic dispersion. Finally, the mixture was subjected to dialysis and centrifugation to remove the free DiR. There was almost no DiR released from the micelles during the experiment, suggesting that DiR could be used to trace the micelles.

The tumor-bearing mice were observed with an *in vivo* imaging system (CRI Inc., Woburn, MA, USA) at a preset time point after intravenous injection with DOX-SS-CSO-SA micelles containing DiR. At the end of the experiment, the mice were sacrificed and various tissues and tumors were collected, weighed, and observed by an *in vivo* imaging system. To calculate the accumulation of DOX-SS-CSO-SA micelles in various tissues as %ID/g (the percentage of the injected dose per gram of tissue), the fluorescent intensity was also read by the imaging system.

2.10. *In Vivo* Antitumor Efficacy. When the tumor volume was approximately 150 mm^3, the nude mice were randomly divided into different groups and treated with various formulations by i.v. injection.

Group 1, 0.9% saline; Group 2, commercial doxorubicin hydrochloride injection (2.0 mg/kg); Group 3, DOX-SS-CSO-SA (2 mg/kg). The injections were continued for 7 days after the first injection. The tumor volume and mice weight were measured every 3 days thereafter. On the 24th day, the mice were sacrificed and tumors were removed and weighed. In addition, the hearts were collected and fixed with formalin for 48 h. After paraffin sectioning, tissue sections were stained with hematoxylin/eosin (H&E) and observed by optical microscopy.

DOI: 10.1021/mp500710x
Mol. Pharmaceutics 2015, 12, 1193−1202

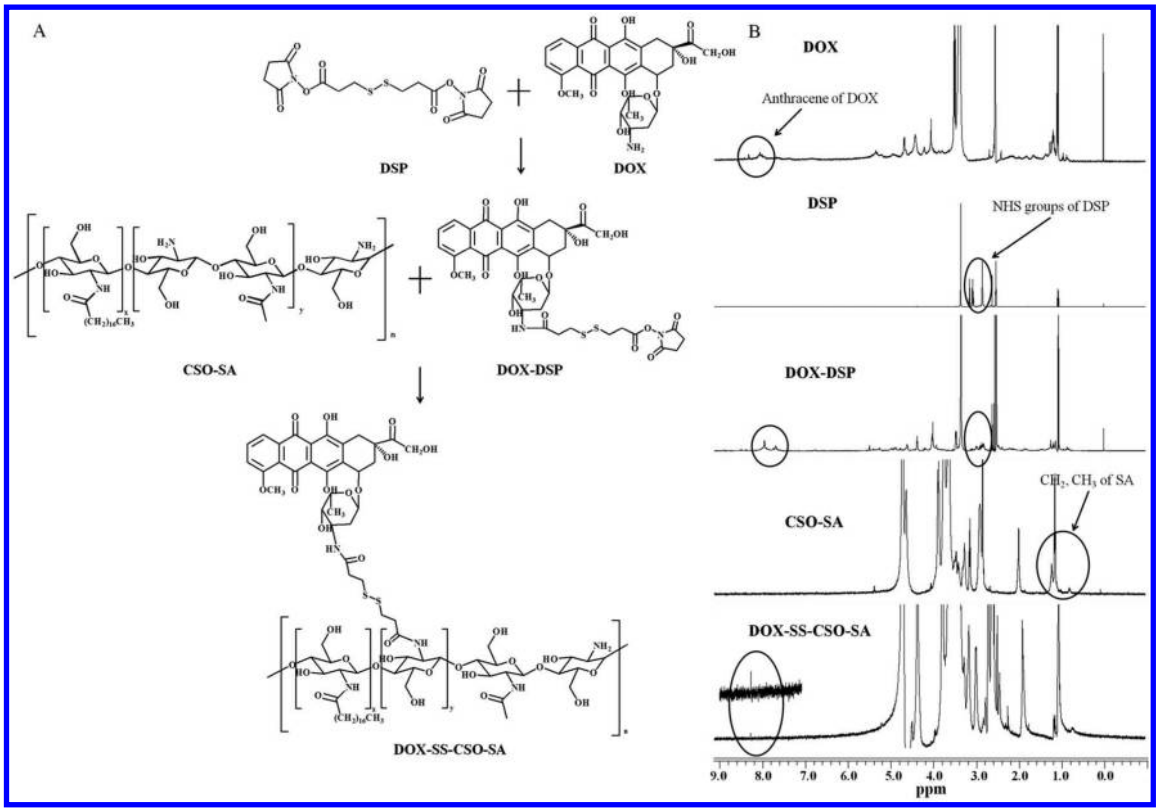

Figure 1. Synthetic route of the DOX-DSP and DOX-SS-CSO-SA (A). ^{1}H NMR spectra of DOX, DSP, DOX-DSP, CSO-SA, and DOX-SS-CSO-SA (B).

2.11. Statistical Analysis. All data represent the mean values ± standard deviation of the independent experiments. Differences between groups were performed using Student's *t*-test (two-tailed), and $p < 0.05$ was considered statistically significant for all cases. Statistically significant differences between pairs of mean values were determined with ANOVA followed by Tukey–Kramer tests. Mean differences with *p*-values < 0.05 were considered statistically significant.

3. RESULTS

3.1. Synthesis of CSO-SA and DOX-SS-CSO-SA. CSO-SA was synthesized by amide reaction of the amino groups of CSO and the carboxyl group of SA catalyzed by EDC. The content of SA on CSO was determined to be 10.03% (molar ratio). DOX-SS-CSO-SA was then synthesized using DSP as the linker. Figure 1A shows the synthetic route for DSP-DOX and DOX-SS-CSO-SA. The structures of products were confirmed by ^{1}H NMR spectra (Figure 1B) and LC/MS spectra (Figure S1). The identity of DSP-DOX could be deduced by the molecular ions: $[M + H]^+$ at m/z 819 in the positive mode. The obtained molecular mass of DSP-DOX product matched with the theoretical value. The area normalization method was used as quantitative analysis of the purity of DSP-DOX, which was 75.8%. After the purification by LC, no molecular ions matching the molecular mass of DSP-DOX-DSP were found in the product. In the ^{1}H NMR spectrum of DSP-DOX, peaks at approximately 8.1 and 2.8 ppm were attributed to the anthracene protons of DOX and the NHS group protons of DSP, respectively.[27] In the spectrum of CSO-SA, peaks at approximately 0.9 and 1.1 ppm belonged to $-CH_3$ and $-CH_2-$ of SA. The spectrum of DOX-SS-CSO-SA was similar to the spectrum of CSO-SA but the small anthracene proton peaks of DOX at approximately 8.2 ppm were found. These results confirmed that DOX-SS-CSO-SA was successfully synthesized. The DOX content in DOX-SS-CSO-SA was measured as 5.5% (weight ratio) by UV spectrophotometer.[24] The weak peaks of DOX in the ^{1}H NMR spectrum from DOX-SS-CSO-SA may result from the low DOX content and poor solubility of DOX in D_2O.

3.2. Characteristics of DOX-SS-CSO-SA. Synthesized DOX-SS-CSO-SA easily self-assembled into micelles in aqueous solution due to the conjugation of the hydrophilic chain (CSO) and hydrophobic segment (SA and DOX).[17] Table 1 shows the characteristics of DOX-SS-CSO-SA. The

Table 1. Characteristics of CSO-SA and DOX-SS-CSO-SA

material	size (nm)	PI[a]	zeta potential (mV)	CMC (μg/mL)
CSO-SA	40.5 ± 4.8	0.401 ± 0.044	32.7 ± 1.1	59.8
DOX-SS-CSO-SA	62.8 ± 5.4	0.266 ± 0.025	21.6 ± 1.2	49.1

[a]PI presents the polydispersity index of the micelle size. The data represent the mean ± standard deviation ($n = 3$).

CMC confirmed the self-aggregation ability of CSO-SA and DOX-SS-CSO-SA.[18,22] As shown in Figure 2A, at low concentration, the fluorescence intensity ratio of the first peak to the third peak (I_1/I_3) in the emission spectra of pyrene remained constant at approximately 1.7. When the concentration increased to form micelles, the I_1/I_3 value sharply decreased as a result of pyrene incorporation into the micelles. The CMC values for DOX-SS-CSO-SA and CSO-SA in DI water was approximately 49.1 and 59.8 μg/mL, respectively, which indicated that the CSO-SA after DOX conjugation had

DOI: 10.1021/mp500710x
Mol. Pharmaceutics 2015, 12, 1193–1202

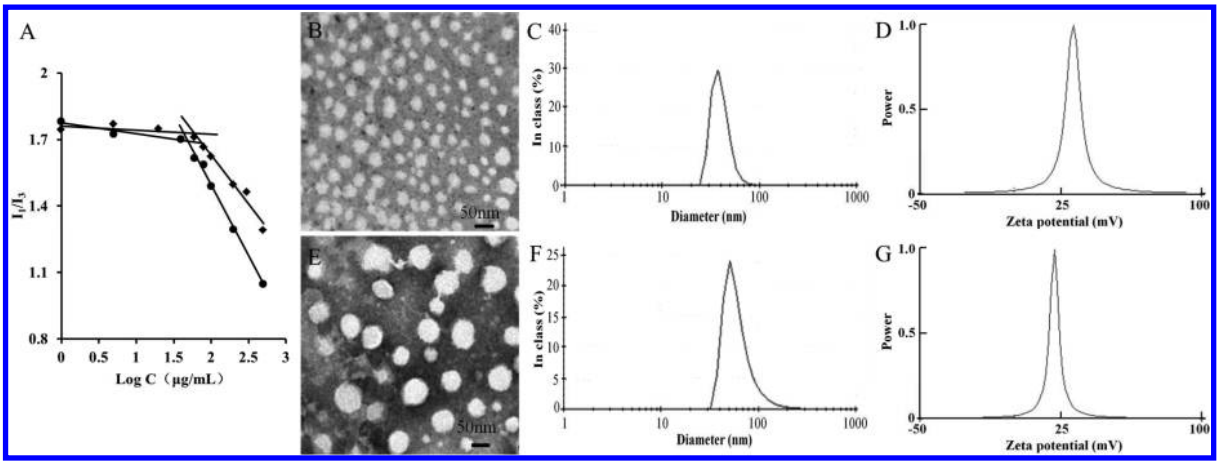

Figure 2. Characteristics of CSO-SA and DOX-SS-CSO-SA. Variations in the fluorescence intensity ratio I_1/I_3 with logarithm concentrations of CSO-SA (♦) and DOX-SS-CSO-SA (●) (A). TEM image (B), size distribution (C), and zeta potential (D) of CSO-SA micelles. TEM image (E), size distribution (F), and zeta potential (G) of DOX-SS-CSO-SA micelles.

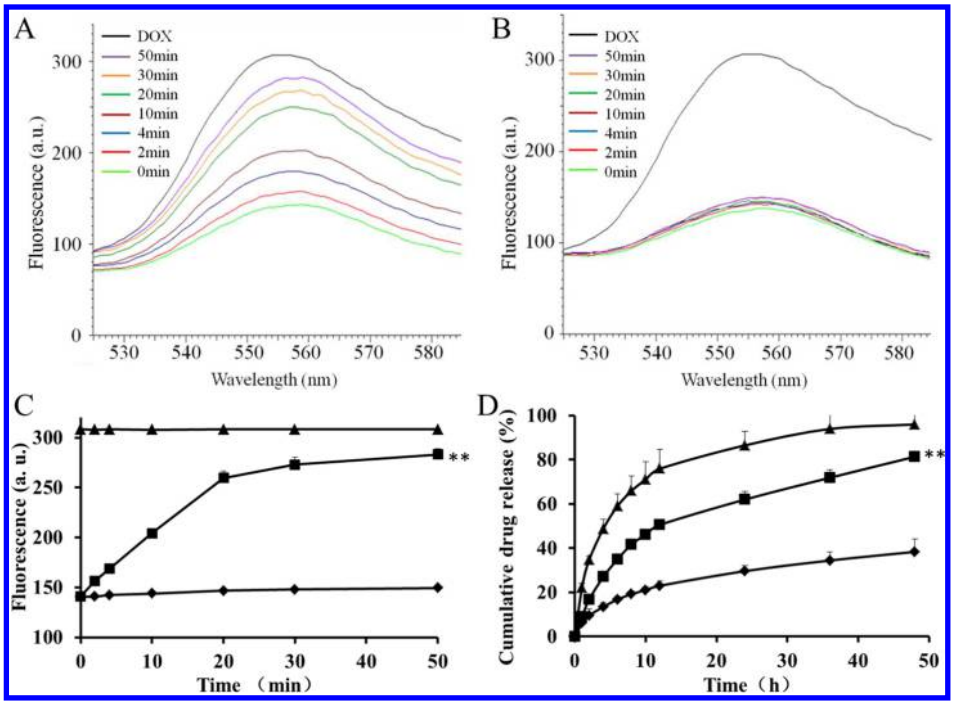

Figure 3. Redox-responsive behavior and the *in vitro* controlled DOX release of DOX-SS-CSO-SA micelles. Fluorescence emission spectra of DOX-SS-CSO-SA micelles after incubation in PBS (pH, 7.4) containing 10 mM DTT (A) or 10 μM DTT (B) at different times. Fluorescence intensity (C) or *in vitro* DOX release profile (D) of DOX-SS-CSO-SA micelles. DOX-SS-CSO-SA micelles in PBS (pH, 7.4) containing 10 mM DTT (■), DOX-SS-CSO-SA micelles in PBS (pH, 7.4) containing 10 μM DTT (♦), and DOX in PBS (pH, 7.4) containing 10 mM DTT (▲). *p < 0.05, **p < 0.01, compared with 10 μM DTT group. The error is the standard deviation from the mean (n = 3).

excellent dispersity and self-assembly ability in aqueous environments.

TEM images, size distributions, and zeta potentials of CSO-SA and DOX-SS-CSO-SA micelles are presented in Figure 2B–G. We found that DOX-SS-CSO-SA micelles were larger in size (62.8 ± 5.4 nm) than CSO-SA micelles (40.5 ± 5.8 nm) as determined by DLS, which was in accordance with the results shown in TEM images. It was obvious that the DOX-SS-CSO-SA micelles had a lower positive zeta potential (21.6 ± 1.2 mV) compared with the CSO-SA micelles (32.7 ± 1.1 mV) due to the decreased amine groups on the micelle surface and enhanced micelle size after DOX conjugation.

3.3. Redox-Responsive Behaviors and *in Vitro* DOX Release. To demonstrate that the disulfide bonds in DOX-SS-CSO-SA micelles are responsive to the reductive environment, the fluorescence emission of DOX-SS-CSO-SA micelles incubated with DTT was measured at different time points. As previously reported, the fluorescence emission of DOX quenches when DOX is covalently conjugated with a polymer, and it recovers when it is separated from polymers.[7,8] The DTT concentrations were set at 10 mM and 10 μM to simulate the intracellular thiol concentration and extracellular level, respectively. As shown in Figure 3A, the fluorescence emission of the DOX-SS-CSO-SA micelle solution increased to a plateau that was close to the fluorescence intensity of free DOX within

DOI: 10.1021/mp500710x
Mol. Pharmaceutics 2015, 12, 1193−1202

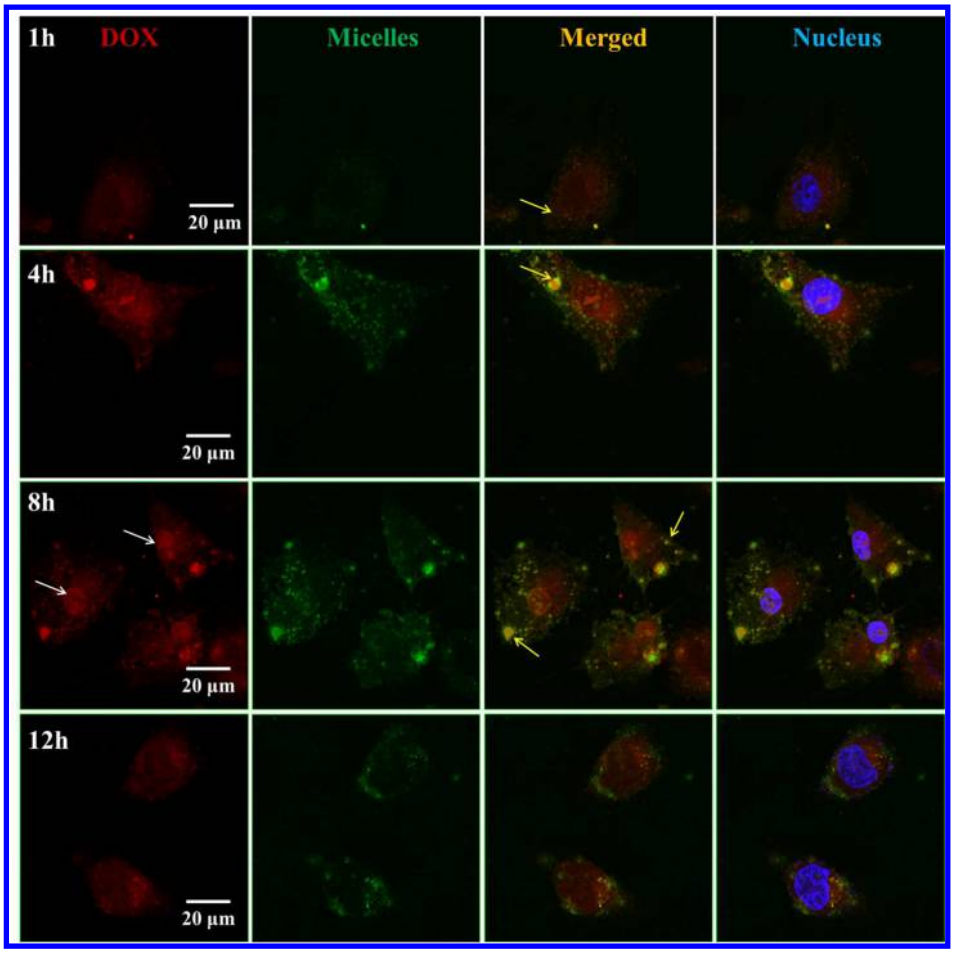

Figure 4. Confocal laser scanning micrographs of MCF-7 cells after incubation with DOX-SS-CSO-SA for 1, 4, 8, and 12 h: DOX (red), FITC-labeled micelles (green), and nuclei stained with Hoechst 33342 (blue).

Table 2. Cytotoxicity of CSO-SA, DOX·HCl, DOX, and DOX-SS-CSO-SA micelles against BEL-7402, MCF-7, and MCF-7/Adr Cells[a]

material	IC_{50}			reversal power
	BEL-7402	MCF-7	MCF-7/Adr	
CSO-SA (μg/mL)	347 ± 32	307 ± 26	488 ± 66	
DOX·HCl (μM)	0.94 ± 0.01	0.57 ± 0.05	67.63 ± 11.64	
DOX (μM)	14.88 ± 1.64	8.10 ± 0.70		
DOX-SS-CSO-SA (μM)	12.45 ± 1.10*	3.59 ± 0.39*	12.28 ± 1.42**	34.7

[a]*p < 0.05, **p < 0.01, compared with DOX·HCl group. The error is the standard deviation from the mean (n = 3).

50 min after incubation in PBS (pH, 7.4) containing 10 mM DTT, which was the result of the cleavage of disulfide linkers and separation of DOX from the polymer. In contrast, no significant increase in fluorescence intensity was observed in PBS (pH, 7.4) containing 10 μM DTT (Figure 3B). In Figure 3C, it is quantitatively shown that the disulfide bonds were rapidly cleaved within 20 min in a reductive environment and that they were stable in a low reductive environment within 50 min (p < 0.05).

In vitro drug release of DOX-SS-CSO-SA in different mediums is shown in Figure 3D. As a control, free DOX was completely released within 48 h. Approximately 38.3% DOX was released from the DOX-SS-CSO-SA micelles within 48 h in media simulating the extracellular thiol concentration (10 μM). However, approximately 81.4% DOX was released within 48 h when the polymer−drug conjugate was incubated in PBS (pH, 7.4), simulating the intracellular thiol concentration (10 mM). The drug release rate of DOX-SS-CSO-SA micelles with 10 mM DTT was significantly faster compared with that of 10 μM of DTT (p < 0.05). These results indicate that DOX-SS-CSO-SA micelles are relatively stable in nonreducing environments, and they are sensitive to intracellular reductive environments, which result in the fast release of DOX.

3.4. Internalization and Intracellular Trafficking. Confocal laser scanning microscopy (CLSM) analysis was performed with MCF-7 cells to investigate the internalization and intracellular trafficking behavior of micelles. In Figure 4, the yellow color (merged, the yellow arrow mark) is an indication for DOX-SS-CSO-SA micelles in which DOX (red fluorescence) did not release from the FITC-conjugated micelles (green fluorescence). When MCF-7 cells were treated with DOX-SS-CSO-SA micelles (DOX content was 5 μg/mL) for 1

DOI: 10.1021/mp500710x
Mol. Pharmaceutics 2015, 12, 1193−1202

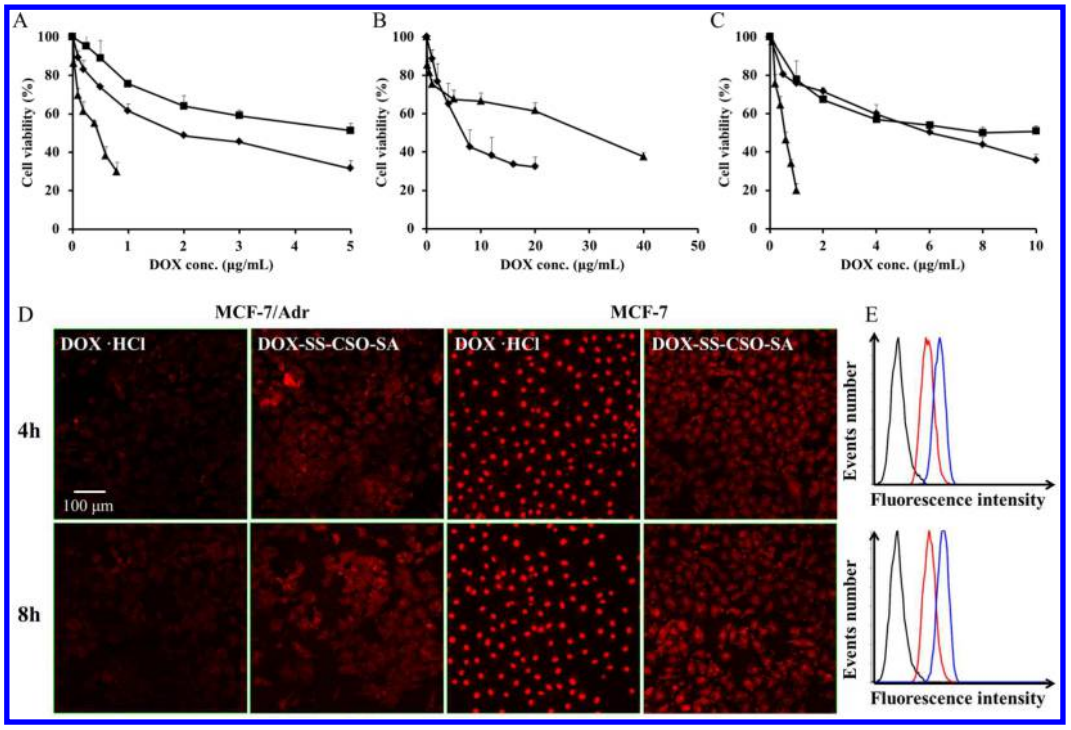

Figure 5. Cytotoxicity of DOX-SS-CSO-SA (♦), DOX·HCl (▲), and DOX (■) against MCF-7 (A), MCF-7/Adr (B), and BEL-7402 (C) cells. Data represent the mean ± standard deviation (n = 3). Fluorescence images of MCF-7 and MCF-7/Adr cells after incubation with DOX·HCl and DOX-SS-CSO-SA micelles (DOX content was 5 μg/mL) for 4 and 8 h, respectively (D). Quantitative cell uptake as analyzed by a flow cytometer into MCF-7/Adr cells incubated with DOX·HCl (red line) and DOX-SS-CSO-SA micelles (blue line) (DOX content was 5 μg/mL) for 4 and 8 h. MCF-7/Adr cells without treatment (black line) are shown as a control (E).

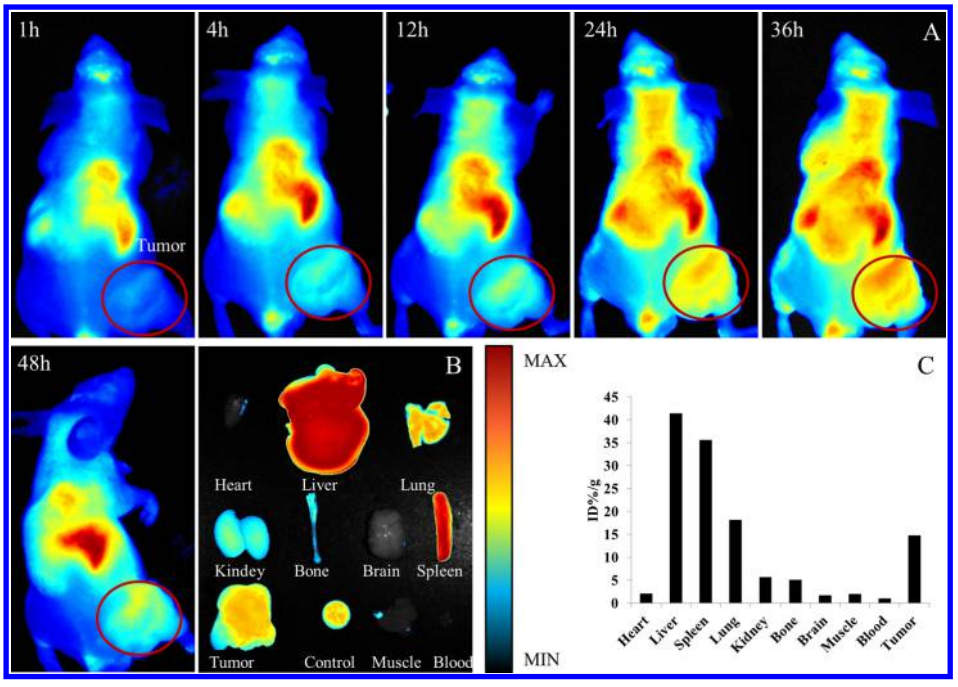

Figure 6. *In vivo* fluorescence images of a tumor-bearing nude mouse at different times after the *i.v.* injection of DOX-SS-CSO-SA micelles encapsulating DiR (A). Fluorescence imaging of various tissues of the mouse at 48 h after *i.v.* injection (B). The accumulation of DOX-SS-CSO-SA micelles in various tissues was calculated as %ID/g (the percentage of the injected dose per gram of tissue). The fluorescent intensity, responding to the amount of the micelles, was read by the imaging system (C).

h, the yellow fluorescence was evident in cells, indicating that the micelles had good internalization capacity. At 4 and 8 h, in merged images, there was green fluorescence from responding micelles without drug but not at 1 h. DOX effectively migrated into the nucleus where it presumably intercalated into DNA, inducing cell death. This process was observed when DOX fluorescence colocalized with the nucleus (labeled with Hoechst 33342, the white arrow marked), while the micelle fluorescence

DOI: 10.1021/mp500710x
Mol. Pharmaceutics 2015, 12, 1193−1202

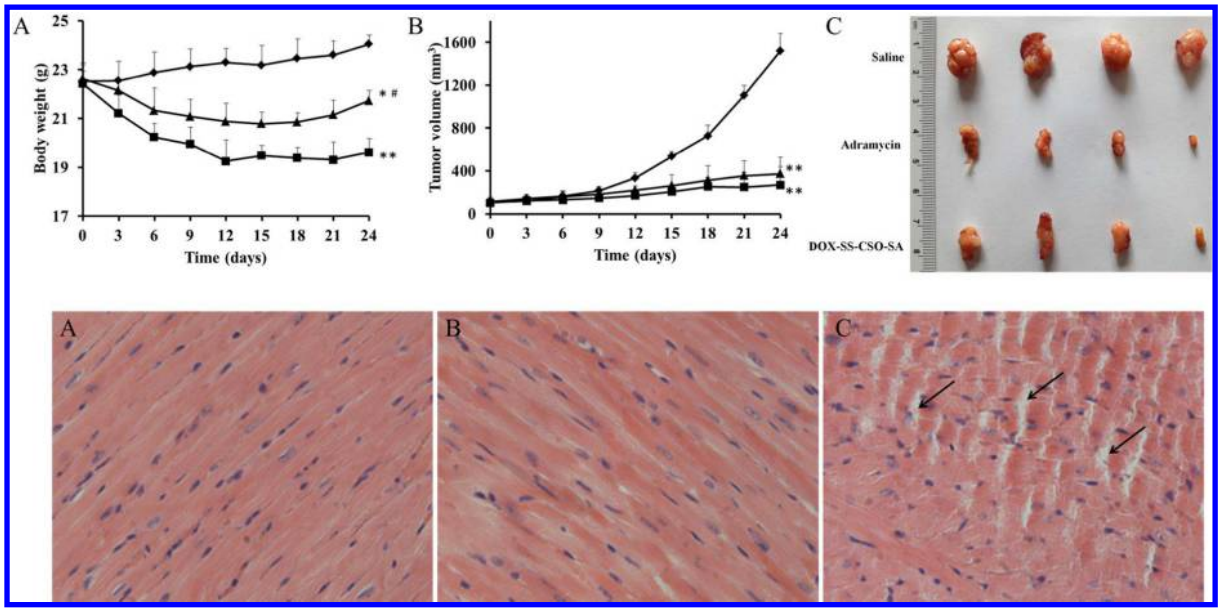

Figure 7. *In vivo* antitumor effect and systemic toxicity of DOX-SS-CSO-SA micelles. Body weight changes (n = 4) (A) and tumor volume changes (n = 4) (B) of BEL-7402 cell tumor-bearing mice treated with saline (♦), adriamycin (■), and DOX-SS-CSO-SA micelles (▲). *p < 0.05, **p < 0.01, compared with saline group. $^{\#}p$ < 0.05, $^{\#\#}p$ < 0.01, compared with adriamycin group. The error is the standard deviation from the mean (n = 4). Excised BEL-7402 solid tumors from different treatment groups on the 24th day (n = 4) (C). Histologic evaluation of the cardiac tissue corresponding to the saline treated group (D), the DOX-SS-CSO-SA micelle treated group (E), and the adriamycin treated group (F).

did not. Dramatic changes in cell and nuclear morphology were observed within 12 h because of tumor cell death. In summary, DOX is rapidly released from redox-sensitive polymer−drug conjugates into cancer cells. DOX then accumulates in target subcellular organelles and induces the death of tumor cells.

3.5. *In Vitro* Cytotoxicity. The *in vitro* cytotoxicity of DOX-SS-CSO-SA was evaluated against MCF-7, MCF-7/Adr, and BEL-7402 cells. DOX base and DOX·HCl served as controls. Previous reports demonstrated that attachment of DOX via a low molecular weight amine group did not reduce the potency of the drug.[28,29] Fifty percent cell growth inhibition (IC_{50}) of BEL-7402, MCF-7, and MCF-7/Adr cells was determined by MTT assay (Table 2). As shown in Figure 5A−C, the IC_{50} values of CSO-SA micelles for BEL-7402, MCF-7, and MCF-7/Adr cells were approximately 347, 307, and 488 μg/mL, respectively, indicating that the micelles have low cytotoxicity. From Table 2 and Figure 5A,C, the IC_{50} value of DOX-SS-CSO-SA micelles is lower than that of DOX (p < 0.05) in BEL-7402 and MCF-7 cells, and the cell viability percentage for both cell lines is reduced with increasing DOX-SS-CSO-SA concentration in the micelles. In MCF-7/Adr cells, the IC_{50} value of DOX·HCl was 118.6-fold higher than that of the MCF-7 cells, which confirmed the DOX resistance of MCF-7/Adr cells. However, the IC_{50} value was only 3.4-fold between the MCF-7/Adr and MCF-7 cells by DOX-SS-CSO-SA. The overcoming ability of drug resistance for DOX-SS-CSO-SA was 34.6. These results indicated that DOX-SS-CSO-SA could overcome the drug resistance of MCF-7/Adr cells.

To investigate the mechanism of how DOX-SS-CSO-SA micelles overcome drug resistance, CLSM analysis with a flow-cytometer was performed to estimate the intracellular DOX concentration in MCF-7 and MCF-7/Adr cells. DOX·HCl served as control. As shown in Figure 5D, after the cells were incubated with 5 μg/mL DOX·HCl for 4 or 8 h, and the DOX concentration in MCF-7/Adr cells was much lower than that in MCF-7 drug-sensitive cells. In contrast, for DOX-SS-CSO-SA micelles, the intracellular DOX concentration was similar in MCF-7 and MCF-7/Adr cells. In addition, in drug resistant cells, the drug concentration of DOX-SS-CSO-SA micelles was significantly higher than that of those in the DOX·HCl group, which was further confirmed by analysis with flow cytometry (Figure 5E).

3.6. *In Vivo* Distribution. Far-red and near-infrared light in the spectral range of 650−900 nm, was a "clear" window for *in vivo* optical imaging because it is separated from the major absorption peaks of organisms.[30] The *in vivo* distribution image of DiR-marked DOX-SS-CSO-SA micelles is shown in Figure 6A. There was an increased accumulation of DOX-SS-CSO-SA micelles in BEL-7402 tumors from 1 to 36 h, and the accumulated amount of micelles in tumors peaked at 36 h. It was indicated that DOX-SS-CSO-SA micelles could passively target tumors, which was attributed to the EPR effect of the nanoscale micelles. To further investigate the distribution of DOX-SS-CSO-SA micelles, organs and tumors were collected, weighed, and observed at 48 h after injection. In Figure 6B,C, we could find that DOX-SS-CSO-SA micelles accumulated in the liver (41.4%, ID/g), spleen (35.5%, ID/g), tumors (14.7%, ID/g), and lungs (18.1%, ID/g). Strikingly, there was nearly no accumulation of DOX-SS-CSO-SA micelles in the heart (2.0%, ID/g).

3.7. *In Vivo* Antitumor Efficacy. The tumor growth inhibitions *in vivo* were performed on the BEL-7402 xenograft tumor bearing nude mice. Commercial preparation adriamycin was used as a positive control. Measurements of changes in body weight (Figure 7A) demonstrated that DOX-SS-CSO-SA micelles are safer than adriamycin. Figure 7B,C illustrates changes in the tumor volume and excised BEL-7402 solid tumors. Both adriamycin and DOX-SS-CSO-SA treatments showed effectively inhibition of tumor growth. The tumor inhibition rate (IR) was 82.7% for adriamycin treatment group and 70.8% for DOX-SS-CSO-SA treatment group. These

DOI: 10.1021/mp500710x
Mol. Pharmaceutics 2015, 12, 1193−1202

results confirmed the efficient suppression ability of tumor growth *in vivo* of DOX-SS-CSO-SA.

In addition, to validate the attenuated doxorubicin-induced cardiac injury of DOX-SS-CSO-SA, the histology and pathology of cardiac tissues from mice with different treatments were observed by pathological sectioning (Figure 7D−F). In Figure 7F, cardiomyocytes from the adriamycin treatment group were scattered and ruptured and had vacuolar degeneration (the arrow mark). In contrast, after treatment with DOX-SS-CSO-SA micelles, the cardiomyocytes (Figure 7E) were maintained the same as the negative control group.

4. DISCUSSION

DOX-SS-CSO-SA was synthesized via amide reactions of the NHS ester groups of DSP between DOX and CSO-SA micelles at physiological pH and room temperature to form amide bonds.[3,4] Thus, DOX was covalently conjugated into CSO-SA micelles via disulfide bonds. The obtained polymer−drug conjugates maintained the properties of physicochemical polymers and easily self-assembled into a core−shell structure in an aqueous environment. Therefore, the polymer−drug conjugates could improve the water solubility of the hydrophobic drug. The reaction between the DOX and CSO-SA was carried out in the H_2O/DMSO solution in which the amino groups of CSO mainly appeared on the surface of the micelles. On the basis of the collision theory, when DOX-DSP solution was added dropwise in the CSO solution, succinyl groups of DOX-DSP preferentially collided with the amino groups on the surface of the micelles and reacted. So part of the hydrophobic DOX may appear on the surface of the micelles. This result could be demonstrated by the fact that the size of the DOX-SS-CSO-SA was larger, and the zeta potential was lower compared with the CSO-SA (Table 1). The structure of DOX-SS-CSO-SA micelles made it possible for DOX to be rapidly released from them in a reducing environment.

Disulfide bonds in the polymer−drug conjugates were introduced as redox-sensitive linkers for intracellular release of DOX,[14] which were rapidly broken by the abundance of intracellular thiols, resulting in DOX separation from micelles and transportation into nuclei (Figures 3 and 4). In contrast, in extracellular fluid or systemic circulation, which has low concentration of thiols, nearly no DOX was leaked from the DOX-SS-CSO-SA. Furthermore, DOX-SS-CSO-SA could passively target to the solid tumor issue due to the EPR effect and reduce nonspecific accumulation in biological systems (particularly in the heart) (Figure 6). Thus, DOX-SS-CSO-SA micelles have high antitumor effects and low toxicity, which could attenuate doxorubicin-induced cardiac injury (Figure 7).

Multiple lines of evidence have demonstrated that the drug resistance in tumor is caused by the overexpression of ATP-binding cassette (ABC) transporters on the cell membrane. As one of the ABC, P-gp is an energy-dependent efflux pump, which could actively efflux cytotoxic agents from the cells.[16] P-gps are large, glycosylated membrane proteins that localize predominantly to the plasma membrane. In the passive diffusion process of internalization, free drug molecules could be easily exported by the Pgp transports near plasma membrane of the resistance cells. Therefore, the DOX concentration in MCF-7/Adr cells was much lower than that in MCF-7 cells (Figure 5D), and in the MCF-7/Adr cells, the viability rate barely changed with an increase in drug concentration from 5 to 20 μg/mL (Figure 5B). Because of the membrane affinity of cationic and special spatial structure of CSO-SA, DOX-SS-CSO-SA entered resistance cells by endocytic pathways. The internalization pathway of DOX-SS-CSO-SA substantially increased the intracellular drug concentration of the drug resistant cells and greatly avoided the efflux of the Pgp transports on plasma membrane.

P-gp and MDR related proteins (MRP1 and MRP4) are ATP-binding cassette transporters, which function as energy-dependent efflux pumps to remove cytotoxic agents from drug resistant cells.[31] DOX-SS-CSO-SA micelles entered cells via endocytosis, which was assumed to reduce the ATP production in drug resistant cells. The decrease of ATP could also reduce the effect of efflux pumps.

Early studies reported that proteins bearing O-linked single or multiple *N*-acetylglucosamine (GIcNAc) moieties were particularly abundant in the cytoplasmic and nucleoplasmic (but not lumenal) sides of nuclear membranes.[32,33] As the monomer structure of chitosan is identical to the GIcNAc, we assumed that CSO-SA may hold the potential to gather into the cell nuclei. Since DOX interacts with DNA in the cell nuclei, the delivery of DOX tends to enrich in the cell nuclei and could substantially increase its efficacy. Thus, DOX-SS-CSO-SA micelles have excellent properties for overcoming the drug-resistance of MCF-7/Adr cells (Table 2 and Figure 5).

5. CONCLUSIONS

We have developed a smart polymer−drug conjugate where DOX is covalently bonded to CSO-SA via disulfide linkage for redox triggered drug release. The polymer−drug conjugate selectively accumulated at tumor sites and showed minor nonspecific accumulation in the heart. After the polymer−drug conjugate rapidly internalized into cancer cells, DOX was rapidly released due to the cleavage of the disulfide bonds mediated by an abundance of free intracellular thiols and then trans-located into nuclei. Our data indicated that the polymer−drug conjugate could overcome MDR *in vitro* by eluding the drug efflux pumps. The polymer−drug conjugate showed a good anticancer effect and low toxicity *in vivo*. All of these results suggest that the polymer−drug conjugate holds certain potentiality for safe and effective cancer therapy.

■ ASSOCIATED CONTENT

Ⓢ Supporting Information

LC/MS analysis and quantitative analysis report. This material is available free of charge via the Internet at http://pubs.acs.org.

■ AUTHOR INFORMATION

Corresponding Author

*E-mail: hufq@zju.edu.cn. Tel: +86-571-88208441. Fax: +86-571-88208439.

Author Contributions

§These authors contributed equally to this work.

Notes

The authors declare no competing financial interest.

■ ACKNOWLEDGMENTS

We are grateful for financial support from National Natural Science Foundation of China (81273442) and Zhejiang Provincial Program for the Cultivation of High-level Innovative Health Talents. We would also like to thank Mrs. Xiaodan Wu from the Analysis Center of Agrobiology and Environmental Science, Zhejiang University for the LC/MS analysis.

DOI: 10.1021/mp500710x
Mol. Pharmaceutics 2015, 12, 1193−1202

REFERENCES

(1) Haag, R.; Kratz, F. Polymer therapeutics: concepts and applications. *Angew. Chem., Int. Ed.* **2006**, *45*, 1198−215.

(2) Bildstein, L.; Dubernet, C.; Couvreur, P. Prodrug-based intracellular delivery of anticancer agents. *Adv. Drug Delivery Rev.* **2011**, *63*, 3−23.

(3) Khandare, J.; Minko, T. Polymer−drug conjugates: Progress in polymeric prodrugs. *Prog. Polym. Sci.* **2006**, *31*, 359−397.

(4) Santra, S.; Kaittanis, C.; Santiesteban, O. J.; Perez, J. M. Cell-specific, activatable, and theranostic prodrug for dual-targeted cancer imaging and therapy. *J. Am. Chem. Soc.* **2011**, *133*, 16680−16688.

(5) Guo, X.; Shi, C.; Wang, J.; Di, S.; Zhou, S. pH-triggered intracellular release from actively targeting polymer micelles. *Biomaterials* **2013**, *34*, 4544−4554.

(6) Etrych, T.; Kovář, L.; Strohalm, J.; Chytil, P.; Říhová, B.; Ulbrich, K. Biodegradable star HPMA polymer-drug conjugates: Biodegradability, distribution and anti-tumor efficacy. *J. Controlled Release* **2011**, *154*, 241−248.

(7) Talelli, M.; Iman, M.; Varkouhi, A. K.; Rijcken, C. J.; Schiffelers, R. M.; Etrych, T.; Ulbrichb, K.; Nostrum, C. F.; Lammersa, T.; Storm, G.; Hennink, W. E. Core-crosslinked polymeric micelles with controlled release of covalently entrapped doxorubicin. *Biomaterials* **2010**, *31*, 7797−7804.

(8) Law, B.; Tung, C. H. Proteolysis: a biological process adapted in drug delivery, therapy, and imaging. *Bioconjugate Chem.* **2009**, *20*, 1683−1695.

(9) Johnson, J. A.; Lu, Y. Y.; Burts, A. O.; Xia, Y.; Durrell, A. C.; Tirrell, D. A.; Grubbs, R. H. Drug-loaded, bivalent-bottle-brush polymers by graft-through ROMP. *Macromolecules* **2010**, *43*, 10326−10335.

(10) Kurtoglu, Y. E.; Navath, R. S.; Wang, B.; Kannan, S.; Romero, R.; Kannan, R. M. Poly(amidoamine) dendrimer-drug conjugates with disulfide linkages for intracellular drug delivery. *Biomaterials* **2009**, *30*, 2112−2121.

(11) Navath, R. S.; Wang, B.; Kannan, S.; Romero, R.; Kannan, R. M. Stimuli-responsive star poly(ethylene glycol) drug conjugates for improved intracellular delivery of the drug in neuroinflammation. *J. Controlled Release* **2010**, *142*, 447−456.

(12) Kuppusamy, P.; Li, H.; Ilangovan, G.; Cardounel, A. J.; Zweier, J. L.; Yamada, K.; Krishna, M. C.; Mitchell, J. B. Noninvasive imaging of tumor redox status and its modification by tissue glutathione levels. *Cancer Res.* **2002**, *62*, 307−312.

(13) Hwang, C.; Sinskey, A. J.; Lodish, H. F. Oxidized redox state of glutathione in the endoplasmic reticulum. *Science* **1992**, *257*, 1496−1502.

(14) Lee, M. H.; Yang, Z.; Lim, C. W.; Lee, Y. H.; Dongbang, S.; Kang, C.; Kim, J. S. Disulfide-cleavage-triggered chemosensors and their biological applications. *Chem. Rev.* **2013**, *113*, 5071−5109.

(15) Takemura, G.; Fujiwara, H. Doxorubicin-induced cardiomyopathy from the cardiotoxic mechanisms to management. *Prog. Cardiovasc. Dis.* **2007**, *49*, 330−352.

(16) Markman, J. L.; Rekechenetskiy, A.; Holler, E.; Ljubimova, J. Y. Nanomedicine therapeutic approaches to overcome cancer drug resistance. *Adv. Drug Delivery Rev.* **2013**, *65*, 1866−1879.

(17) Hu, F. Q.; Zhao, M. D.; Yuan, H.; You, J.; Du, Y. Z.; Zeng, S. A novel chitosan oligosaccharide-stearic acid micelles for gene delivery: properties and in vitro transfection studies. *Int. J. Pharm.* **2006**, *315*, 158−166.

(18) Li, J.; Huo, M.; Wang, J.; Zhou, J. P.; Mohammad, J. M.; Zhang, Y. L.; Zhu, Q. N.; Waddad, A. Y.; Zhang, Q. Redox-sensitive micelles self-assembled from amphiphilic hyaluronic acid-deoxycholic acid conjugates for targeted intracellular delivery of paclitaxel. *Biomaterials* **2012**, *33*, 2310−2320.

(19) Yan, J.; Du, Y. Z.; Chen, F. Y.; You, J.; Yuan, H.; Hu, F. Q. Effect of Proteins with Different Isoelectric Points on the Gene Transfection Efficiency Mediated by Stearic Acid Grafted Chitosan Oligosaccharide Micelles. *Mol. Pharmaceutics* **2013**, *10*, 2568−2577.

(20) Zhao, M. D.; Hu, F. Q.; Du, Y. Z.; Yuan, H.; Chen, F. Y.; Lou, Y. M.; Yu, H. Y. Coadministration of glycolipid-like micelles loading cytotoxic drug with different action site for efficient cancer chemotherapy. *Nanotechnology* **2009**, *20*, 055102.

(21) You, J.; Wang, Z.; Du, Y. Z.; Yuan, H.; Zhang, P.; Zhou, J.; Liu, F.; Li, C.; Hu, F. Q. Specific tumor delivery of paclitaxel using glycolipid-like polymer micelles containing gold nanospheres. *Biomaterials* **2013**, *34*, 4510−4519.

(22) Hu, F. Q.; Ren, G. F.; Yuan, H.; Du, Y. Z.; Zeng, S. Shell cross-linked stearic acid grafted chitosan oligosaccharide self-aggregated micelles for controlled release of paclitaxel. *Colloids Surf. B* **2006**, *50*, 97−103.

(23) Kohori, F.; Yokoyama, M.; Sakai, K.; Okano, T. Process design for efficient and controlled drug incorporation into polymeric micelle carrier systems. *J. Controlled Release* **2002**, *78*, 155−163.

(24) Nogusa, H.; Yano, T.; Okuno, S.; Hamana, H.; Inoue, K. Synthesis of carboxymethylpullulan-peptide-doxorubicin conjugates and their properties. *Chem. Pharm. Bull.* **1995**, *43*, 1931−1936.

(25) Lee, K.; Kwon, I.; Kim, Y. H.; Jo, W.; Jeong, S. Preparation of chitosan self-aggregates as a gene delivery system. *J. Controlled Release* **1998**, *51*, 213−220.

(26) Zhou, C.; Shen, P.; Cheng, Y. Quantitative study of the drug efflux kinetics from sensitive and MDR human breast cancer cells. *Biochim. Biophys. Acta* **2007**, *1770*, 1011−1020.

(27) Tanaka, K.; Kitamura, N.; Chujo, Y. Heavy metal-free 19F NMR probes for quantitative measurements of glutathione reductase activity using silica nanoparticles as a signal quencher. *Bioorg. Med. Chem.* **2012**, *20*, 96−100.

(28) Garsky, V. M.; Lumma, P. K.; Feng, D. M.; Wai, J.; Ramjit, H. G.; Sardana, M. K.; Oliff, A.; Jones, R. E.; DeFeo-Jones, D.; Freidinger, R. M. The synthesis of a prodrug of doxorubicin designed to provide reduced systemic toxicity and greater target efficacy. *J. Med. Chem.* **2001**, *44*, 4216−4224.

(29) Zou, P.; Yu, Y.; Wang, Y. A.; Zhong, Y.; Welton, A.; Galbán, C.; Wang, S. M.; Sun, D. X. Superparamagnetic iron oxide nanotheranostics for targeted cancer cell imaging and pH-dependent intracellular drug release. *Mol. Pharmaceutics* **2010**, *7*, 1974−1984.

(30) Ntziachristos, V.; Bremer, C.; Weissleder, R. Fluorescence imaging with near-infrared light: new technological advances that enable in vivo molecular imaging. *Eur. Radiol.* **2003**, *13*, 195−208.

(31) Hu, F. Q.; Liu, L. N.; Du, Y. Z.; Yuan, H. Synthesis and antitumor activity of doxorubicin conjugated stearic acid-g-chitosan oligosaccharide polymeric micelles. *Biomaterials* **2009**, *30*, 6955−6963.

(32) Holt, G. D.; Hart, G. W. The subcellular distribution of terminal n-acetylglucosamine moieties. *J. Biol. Chem.* **1986**, *17*, 8049−8057.

(33) Holt, G. D.; Snow, C. M.; Senior, A.; Haltiwanger, R. S.; Gerace, L.; Hart, G. W. Nuclear pore complex glycoproteins contain cytoplasmically disposed o-Linked n-acetylglucosamine. *J. Cell Biol.* **1987**, *104*, 1157−1164.

DOI: 10.1021/mp500710x
Mol. Pharmaceutics 2015, 12, 1193−1202